

Journal of Biomedical Optics

SPIDigitalLibrary.org/jbo

Transverse chemical interface detection with coherent anti-Stokes Raman scattering microscopy

Sophie Brustlein
David Gachet
Franck Billard
Hervé Rigneault

Transverse chemical interface detection with coherent anti-Stokes Raman scattering microscopy

Sophie Brustlein, David Gachet,* Franck Billard,† and Hervé Rigneault

Aix-Marseille Université, Domaine Universitaire Saint-Jérôme, Institut Fresnel, Mosaic group, CNRS UMR 6133, École Centrale de Marseille, 13397 Marseille cedex 20, France

Abstract. Transverse “chemical” interfaces are revealed with a conventional two beam narrowband coherent anti-Stokes Raman scattering microscopy setup in a collinear configuration. The exciting “pump” and “Stokes” beams are focused on the sample in two opposite directions. The subtraction of the two generated anti-Stokes signals gives rise to a signal that is directly proportional to the pure Raman spectrum of the resonant medium. This property is used to highlight an interface between glass and *N,N*-dimethylformamide (DMF) and recover the pure Raman spectrum of DMF around its 1408 cm^{-1} vibrational band. © 2011 Society of Photo-Optical Instrumentation Engineers (SPIE). [DOI: 10.1117/1.3606574]

Keywords: coherent anti-Stokes Raman scattering; Raman; nonresonant background; microscopy.

Paper 11190R received Apr. 14, 2011; revised manuscript received Jun. 9, 2011; accepted for publication Jun. 13, 2011; published online Aug. 5, 2011.

1 Introduction

Coherent Raman microscopy has proved to be a valuable contrast for fast label-free chemically resolved analysis of biological samples.^{1,2} Coherent anti-Stokes Raman scattering (CARS)^{3,4} and stimulated Raman scattering (SRS)^{2,5-7} are now two common nonlinear contrasts for probing vibrational resonances. CARS and SRS are two third-order nonlinear processes whereby two so-called pump and Stokes frequency-shifted waves interact into the sample. In SRS, the molecular vibrations specific to the sample induce loss and gain over the pump and Stokes beams, respectively. In CARS, these vibrations enhance the blueshifted so-called anti-Stokes signal. While the CARS signal detection is made easier due to this frequency-shift, its molecular specificity is affected by the presence of a nonresonant electronic background that interferes coherently with the resonant vibrational signal. Time-resolved⁸ and optical heterodyne⁹ detection schemes, as well as spectral phase control,^{10,11} frequency-modulation,¹² or vibrational phase contrast¹³ have proved as valuable background-free techniques, nonetheless at the price of increased experimental complexity. On the other hand, polarization sensitive¹⁴ and Epi-CARS¹⁵ detection schemes suppress efficiently this nonresonant background at the price of far reduced detected signal. The interplay between the resonant and coherent nature of CARS makes the signal formation a complex process.¹⁶ Recent works have been devoted to the study of CARS signal generation near interfaces and to the development of techniques sensitive to “chemical” edges.¹⁷⁻²⁰ In a previous work, we demonstrated background-free CARS spectroscopy of

a sample when it makes an interface with a nonresonant medium perpendicular to the optical axis (transverse interface).²¹ For this task, one has to acquire two CARS spectra, the former at the original interface, the latter after permutation of the two media. This technique has mainly been limited by its poor signal-to-noise ratio (SNR) due to the successive acquisition of spectra and restricted to symmetrical samples.²² In this letter, we give at first a simple explanation of the underlying physics at work in term of two-wave interferences. This simple view is supported by full three-dimensional computation. We then extend the capability of this technique to CARS microscopy without the need of permuting the two media. Instead we use a mirror to reflect the excitation CARS beams (that have already crossed the sample) to focus them back on the sample itself. With this simple scheme, we demonstrate experimentally highlighting of transverse chemical interfaces and background-free Raman spectroscopy of test samples with an improved SNR as compared to our previous work.²¹

2 From CARS to Raman Spectrum

The situation that will be studied through the paper is shown in Fig. 1(a) as a reminder. Two resonant and nonresonant medium are separated by a transverse interface. Their third-order nonlinear susceptibilities are given by $\chi_1^{(3)} = \chi_{1R}^{(3)} + \chi_{1NR}^{(3)}$ and $\chi_2^{(3)} = \chi_{2NR}^{(3)}$, respectively. In a first configuration (α -problem), the resonant medium (medium 1) lies in the upper half-space ($z > 0$) and the nonresonant medium lies in the lower one ($z < 0$). In a second configuration the relative positions of medium 1 and 2 are flipped (β -problem). In both configurations, the pump and Stokes beams are focused on the interface. As a result, the CARS active volume overlap both with medium 1 and 2. The anti-Stokes (CARS) signals I_α^{Fwd} and I_β^{Fwd} generated in the direction of propagation of the pump and Stokes beams (forward direction, noted Fwd) in both configurations result from the interference of the anti-Stokes fields generated

*Current address: Aix-Marseille Université, Centre Interdisciplinaire des Nanosciences de Marseille (CINaM), CNRS UPR 3118, Campus de Luminy, Case 913, 13288 Marseille Cedex 9, France.

†Current address: Université de Bourgogne, Institut Carnot de Bourgogne, UMR CNRS 5209, Département “Optique, interaction Matière-Rayonnement,” 9 Avenue Savary, B.P. 47 870, 21078 Dijon Cedex, France.

Address all correspondence to: Domaine Universitaire Saint-Jérôme, Institut Fresnel, Marseille, 13397 Cedex 20, France. Tel: +33 4 91 28 80 49; E-mail: herve.rigneault@fresnel.fr.

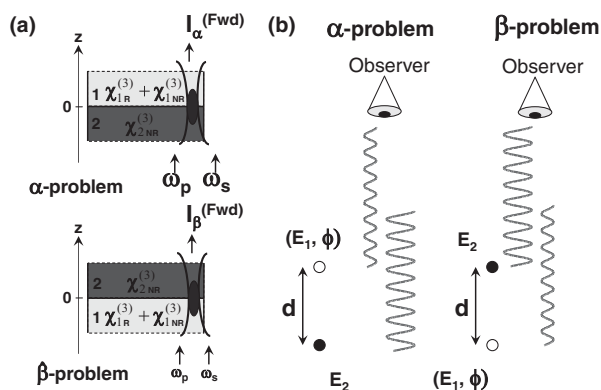


Fig. 1 (a) CARS signal generation near a transverse interface between a resonant and a nonresonant medium. α -problem: the resonant medium lies in the upper half-space ($z > 0$); β -problem: the resonant medium lies in the lower half-space ($z < 0$). (b) Analogy with a two-wave interference experiment.

by medium 1 and 2. Due to the vibrational resonance induced in medium 1, the anti-Stokes field generated by this medium is out of phase with the excitation²³ by a phase shift of ϕ . The situation is in fact analogous to the two-wave interference problem depicted in Fig. 1(b) whereby an observer detects the interference pattern generated by two coherent sources separated by a distance d . The value of d has little importance on the physical effect highlighted here excepted it has to be nonzero (the two sources are not superimposed since they are located in medium 1 and 2, respectively). In the first case (α -problem), the intensity I_α detected by the observer equals

$$I_\alpha = |E_1|^2 + |E_2|^2 + 2|E_1||E_2| \cos\left(\frac{2\pi d}{\lambda} - \phi\right), \quad (1)$$

where E_1 and E_2 are the fields (with wavelength λ) generated by sources 1 and 2, respectively, and ϕ is the phase shift of source 1 with respect to source 2. The additional phase shift term $2\pi d/\lambda$ accounts for geometrical effects. In the second case (β -problem), where the roles of sources 1 and 2 have been permuted, the detected intensity I_β writes

$$I_\beta = |E_1|^2 + |E_2|^2 + 2|E_1||E_2| \cos\left(\frac{2\pi d}{\lambda} + \phi\right). \quad (2)$$

Only the phase shift ϕ introduces a difference in the interference terms in Eqs. (1) and (2). To go further, we proceed to the intensity difference between the Fwd-CARS signals generated at the interfaces for the α and β problems. In the simple two-wave interference model, the intensity difference $\Delta I = I_\alpha - I_\beta$ writes

$$\Delta I = -4|E_1||E_2| \sin\left(\frac{2\pi d}{\lambda}\right) \sin(\phi). \quad (3)$$

If one notes that $|E_1| \sin(\phi) = \text{Im}[E_1]$, it can be readily seen that the intensity difference is proportional to the imaginary part of the field emitted by source 1 (the resonant medium). It can be shown²² that this simple property can be directly transposed to the anti-Stokes signal difference $\Delta I_{\text{as}} = I_\alpha^{\text{Fwd}} - I_\beta^{\text{Fwd}}$ following

$$\Delta I_{\text{as}} \propto 4\chi_{2\text{NR}}^{(3)} \text{Im}\left[\chi_{1\text{R}}^{(3)}\right]. \quad (4)$$

According to our previous study, this expression shows that the anti-Stokes signal difference is proportional to the pure Raman spectrum of the resonant medium.²¹ Similar conclusions have been drawn in the case of an axial “chemical” interface.²⁰

3 Numerical Simulations

We illustrate this basic property of two-wave interferences in the case of the CARS imaging using a three-dimensional full-vectorial model of the CARS emission.^{16,22} In the following numerical examples, the pump and Stokes lasers are focused into the sample through a 1.2 numerical aperture (NA) objective lens and the sample, consisting of a resonant and a nonresonant medium, is raster-scanned. The resonant medium is excited around a unique vibrational resonance with a Lorentzian lineshape $\chi_{1\text{R}}^{(3)} = a/[\omega_p - \omega_s - \Omega_R + i\Gamma]$, where a denotes the oscillator strength of the resonance, $(\omega_p - \omega_s) - \Omega_R$ the detuning to the vibrational resonance, and Γ the half width at half maximum of the vibrational resonance. We assume that the nonresonant part $\chi_{1\text{NR}}^{(3)}$ of $\chi_1^{(3)}$ has the same amplitude as its resonant part $\chi_{1\text{R}}^{(3)}$ ($\chi_{1\text{NR}}^{(3)} = -a/\Gamma$). Finally, the nonresonant medium is assumed to be strongly nonresonant ($\chi_{2\text{NR}}^{(3)} = 2\chi_{1\text{NR}}^{(3)}$). Although quite unusual, this assumption is made to stress the robustness of the method to a strong nonresonant environment.

First, in Fig. 2 we consider a resonant bead surrounded by a nonresonant medium. In this example, the Fwd-CARS signal is collected with a 0.5 NA objective lens. The bead locally makes transverse interfaces with the surrounding nonresonant medium on positions marked as “ α ” and “ β .” On resonance [Fig. 2(a)], the Fwd-CARS signals generated at the lower (α mark) and upper (β mark) interfaces are asymmetric. This asymmetry is better viewed in Fig. 2(c), (upper curve). The profile of the bead is deformed due to interference effects between the resonant bead (whose nonlinear susceptibility $\chi_1^{(3)}$ carries a phase shift ϕ as compared to the surrounding nonresonant medium’s $\chi_2^{(3)}$), and the surrounding nonresonant medium. On the other hand, the Fwd-CARS image of the bead taken off resonance [Fig. 2(b)] is symmetric. The Fwd-CARS signals generated at the lower (α mark) and upper (β mark) interfaces are identical as the phase shift vanishes ($\phi = 0$). The profile of the bead is now symmetric, as shown in Fig. 2(c), (blue curve). The bead z -profile asymmetry observed at resonance is the key effect that makes the α and β interface CARS responses different.

As a second example, we reconsider the initial problem of a transverse interface that separates a resonant and a nonresonant medium. The particular configuration depicted in Fig. 3(a), whereby the β -problem is reached from the α -problem by switching the direction of propagation of the pump and Stokes beams without flipping the sample, is compatible with microscopy applications. In Fig. 3(b), where we have reported data from Ref. 21, are shown the spectral evolution of the Fwd-CARS signals for the α - and β -problems, together with their difference, as a function of the normalized Raman resonance detuning $\zeta = (\omega_p - \omega_s - \Omega_R)/\Gamma$. As previously reported in Ref. 21, the difference recovers the imaginary part of the nonlinear susceptibility $\chi_1^{(3)}$ of the resonant medium (being its Raman spectrum). In addition, in Fig. 3(c) are shown the evolution of the Fwd-CARS signals for the α - and β -problems when the excitation scans the interface. The difference of signals highlights the

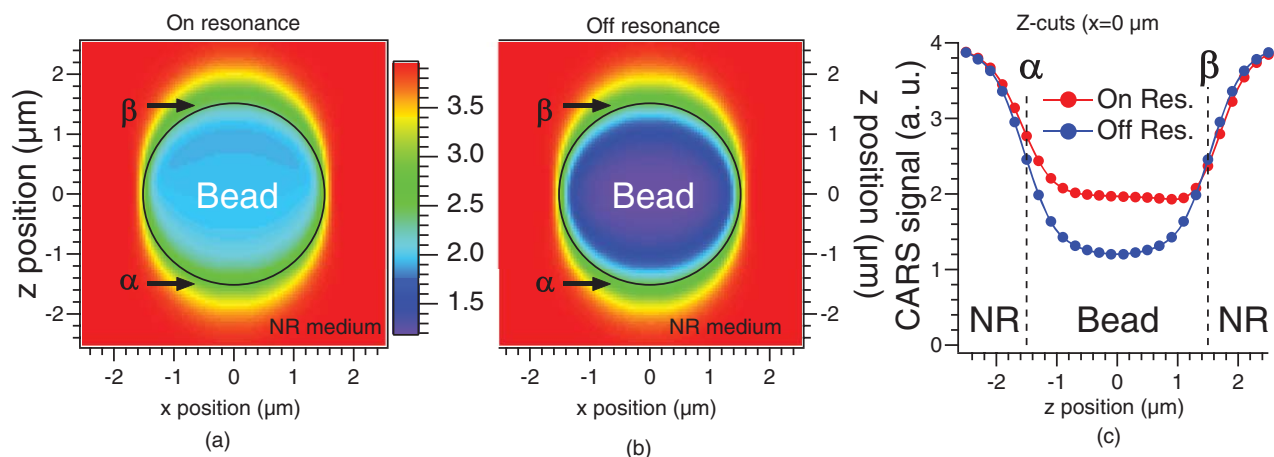


Fig. 2 Fwd-CARS images of a 3 μm bead embedded in a purely nonresonant medium. The bead is on (a) or off (b) Raman resonance. For the bead, the probed Raman line is assumed to be Lorentzian following $\chi_{1R}^{(3)} = a/[\omega_p - \omega_s - \Omega_R + i\Gamma]$ and $\chi_{1NR}^{(3)} = -a/\Gamma$. For the nonresonant surrounding medium, $\chi_{2NR}^{(3)} = 2\chi_{1NR}^{(3)}$. NA of the objectives: 1.2 for the excitation and 0.5 for the collection.

interface, thus emphasizing the applicability of this technique to microscopy.

4 Experiments

In order to apply this property in CARS microscopy, and thus to be able to highlight transverse chemical interfaces, one has to switch between the α - and β -problems. A first solution consists in imaging the interface once, then flipping the sample before acquiring a second image. In practice, this solution is incompatible with most samples and is handicapped by a low SNR due to two successive image acquisitions.²¹ A more elegant solution consists in switching the excitation beams, as already mentioned

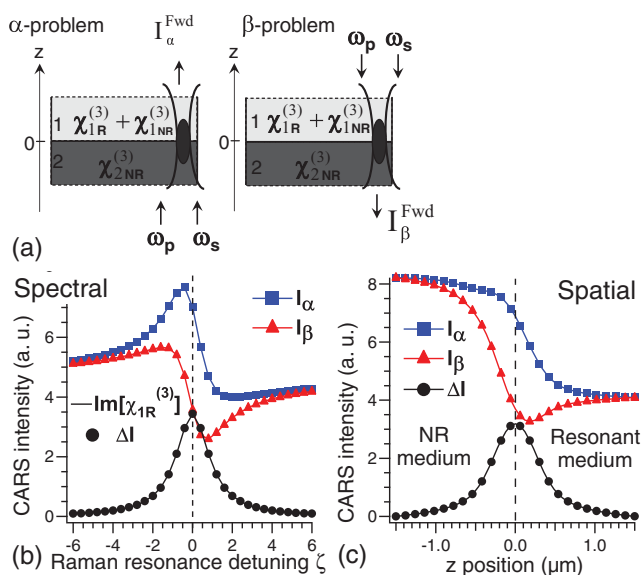


Fig. 3 (a) Scheme of the α - and β -problems when the excitation is reversed. [(b) and (c)] CARS signals emitted for the α (I_α , squares) and β (I_β , triangles) problems versus (a) the normalized Raman resonance detuning ζ for a centered focus ($z = 0$) and (b) the focus shift z to the interface for Raman peak ($\zeta = 0$). ΔI (black dots): signal difference $I_\alpha - I_\beta$; solid line in (b) is $\text{Im}[\chi_{1R}^{(3)}]$. The numerical parameters are the same as in Fig. 2.

in Sec. 3. As depicted in Fig. 4(b), this is achievable in a symmetric configuration where the excitation beams are focused first under a collinear geometry on the interface (α -problem), before being reflected by a mirror to be re-focused a second time on the interface in the opposite direction (β -problem). Such a scheme leaves the sample fixed and insures the simultaneous acquisition of the I_α^{Fwd} and I_β^{Fwd} signals, a feature that greatly enhances the SNR. A schematic of our CARS microscopy setup is depicted in Fig. 4(a). Briefly, two picosecond (3 ps) pump ($\lambda_p = 726 \text{ nm}$) and Stokes (λ_s ranging between 804 and 813 nm) beams, provided by two pulsed pumped (3.8 MHz) synchronized Ti:sapphire oscillators, overlap in a collinear geometry. Two similar objective lenses (then referred as “objective 1” and “objective 2”) are disposed before and after the sample of interest, respectively. In the α -problem, objective 1 focuses the pump and Stokes beams on the sample and objective 2 collects the Fwd-CARS signal generated into the sample and collimates the transmitted pump

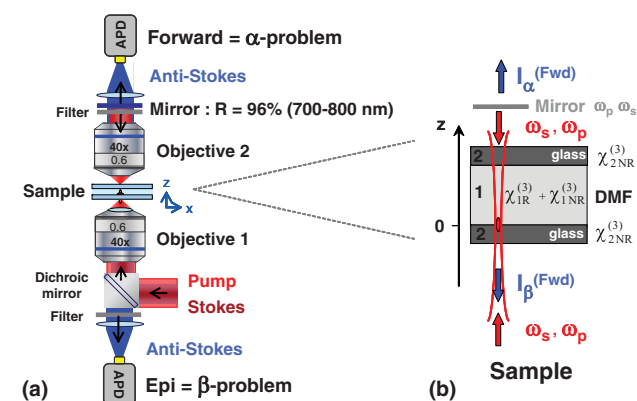


Fig. 4 Experimental scheme. (a) Objectives 1 and 2 are disposed in a symmetric configuration. α -problem: Objective 1 focuses the pump and Stokes beams on the sample and objective 2 collects the Fwd-CARS signal and the pump and Stokes beams. β -problem: Objective 2 focuses the pump and Stokes beams reflected by the mirror on the same point in the sample and objective 1 collects the Fwd-CARS signal generated into the sample. (b) APD properties of the sample. DMF is embedded between two microscope cover slips (glass). The mirror is transparent for the CARS signal but reflects the pump and Stokes beams.

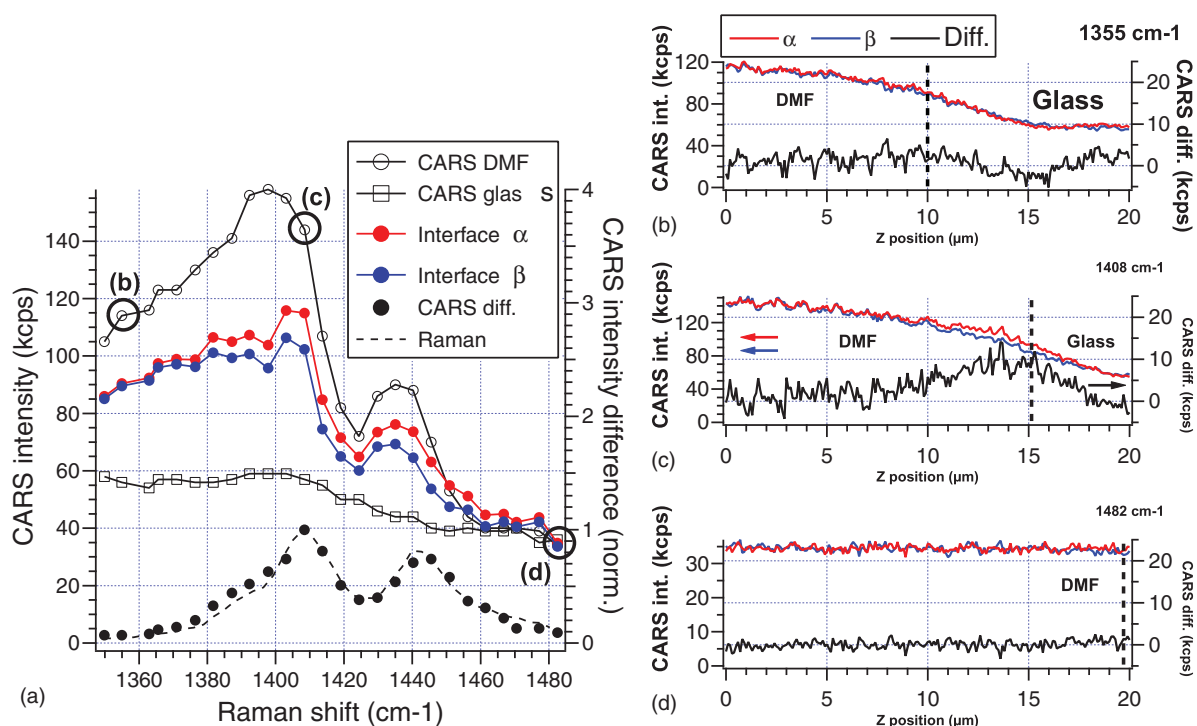


Fig. 5 (a) Raw CARS spectra in bulk DMF (open circles) and glass (squares) and CARS spectra acquired at the DMF/glass interface (α -problem; β -problem) together with their difference (close circles). On the same graph is plotted the experimental DMF spontaneous Raman spectrum (cw excitation at 633 nm). [(b)–(d)] z-scans (α -problem; β -problem) of the DMF/glass interface together with their difference (bottom curve black) before (b), on (c), and after (d) Raman resonances of the DMF. For CARS experiments pump and Stokes power are 10 mW, integration time 10 ms, Stokes wavelength is scanned manually.

and Stokes beams. An interference mirror ($R = 96\%$ on the 700 to 800 nm range) reflects the pump and Stokes beams, and transmits the anti-Stokes signal that is detected by an avalanche photodiode (APD) working in photon counting regime. In the β -problem, the roles of objectives 1 and 2 are swapped. Objective 2 focuses the reflected pump and Stokes beams on the same focal point in the sample, and objective 1 collects the Fwd-CARS signal generated in the sample, that is then detected by a second APD. We found that the time overlap between the pump and Stokes beams are not changed between the first focusing by objective 1 and the second one by objective 2 after reflection by the interference mirror.

5 Results

As a proof-of-principle experiment, we have studied a sample consisting of *N,N*-dimethylformamide (DMF) sandwiched between two microscope cover slips [Fig. 4(b)]. The frequency difference between the pump and Stokes lasers was tuned over the 1350 to 1480 cm⁻¹ region. In this spectral range, DMF exhibits a vibrational band while the microscope cover slips are purely nonresonant [Fig. 5(a)]. The interface between the lower microscope cover slip and the DMF was scanned in the z -direction on the 1350 to 1480 cm⁻¹ region, and the α and β anti-Stokes signals were acquired simultaneously [Figs. 5(b)–5(d)]. We have calibrated the response of the two APDs by acquiring the CARS signals in bulk DMF. When the pump and Stokes beams are focused on the interface, we have checked in the case of the α -problem that the backward emitted CARS sig-

nal is 2 orders of magnitude lower than the Fwd-CARS signal. It thus insures that the signals detected by both APDs are the Fwd-CARS signals generated in the α - and β -problems. When the frequency difference is tuned before the DMF vibrational resonance, the detected α and β CARS signals smoothly change across the interface between the highly emissive DMF (left part) and the glass (right part). However, for each z -position both signals are identical and the signal difference fluctuates around zero so that the interface is not highlighted [Fig. 5(b)]. The situation is different on DMF resonance (1355 cm⁻¹). The detected α and β CARS signals are identical only far away from the interface. In the vicinity of the interface, they split and their difference is nonzero, thus highlighting the interface [Fig. 5(c)]. The half-width at half-maximum of the signal difference is around 6 μ m, a value compatible with the axial extension of an excitation volume generated after focusing through a 0.6 NA objective lens. After the DMF resonance (1355 cm⁻¹), the CARS signals generated in the DMF and the glass are the same and the signal difference is zero all along the z -scan. The drift of the interface during the experiment is due to mechanical instabilities in the setup.

For each Raman shift, the α and β CARS signals, together with the CARS signal difference, have been integrated over 3 μ m around the interface. This operation allows us to reconstruct the spectra plotted in Fig. 5(a). As expected, the α and β spectra are similar far away from the DMF resonance but exhibit a difference on resonance. The CARS signal difference spectrum (filled circles) can be superimposed on the pure Raman spectrum of DMF (dashed lines) perfectly. For comparison, the

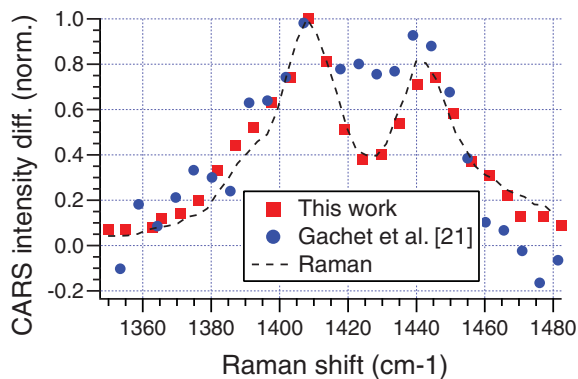


Fig. 6 Comparison between the Raman spectra of DMF, on the 1350 to 1480 cm^{-1} region, recovered by the beam reversal scheme (present work, squares) and our previous sequential spectral acquisition scheme (Ref. 21, dots).

CARS spectra of the DMF (open circles) and the glass (open squares) obtained in the bulk have been plotted. They allow to appreciate the ability of our technique to recover pure Raman spectra with a good SNR. The DMF Raman spectrum found here almost perfectly matches the Raman spectrum, a situation that was far to be reached in Ref. 21 where the α and β signals were recorded sequentially at two distinct interfaces. To appreciate the SNR improvement introduced by this beam reversal scheme, we plot in Fig. 6 the recovered Raman spectra obtained here and with the sequential spectral acquisition scheme introduced in our previous work.²¹

6 Conclusion

The beam reversal technique we have presented in this work allows to highlight transverse chemical interfaces and to perform background-free Raman spectroscopy of transparent and nonscattering media with a conventional narrow band CARS microscope. Compared to the first realization of this concept,²¹ the simultaneous acquisition of the two signals makes this differential approach far less noisy and compatible with microscopy applications. The very origin of the method has been simply interpreted in terms of two-wave interferences between the resonant and the nonresonant media, and the full electromagnetic calculation at the bead interface illustrated in Fig. 2 gives a clear view of the effect. The presented scheme has the ability to generate a background-free CARS signal with the surprising ability of performing an heterodyne detection (with the nonresonant medium) through a simple intensity subtraction. In particular, when implemented in multiplex CARS²⁴ the method has a strong potential for fast chemical analysis in microfluidic devices.²⁵ When combined with our recently published method to detect background free axial interface,²⁰ the present technique shows potential to image biological samples featuring both axial and transverse interfaces.²⁶ The present technique and the one reported in Ref. 20 use interference between the resonant sample and the nonresonant surrounding medium when the active CARS spot is located right at the interface. As demonstrated for axial interfaces, such techniques are viable for interfaces with small refractive index mismatch as the ones encountered in cell imaging.

Acknowledgments

The authors would like to thank Dr. Jérôme Wenger for spontaneous Raman measurements and Dr. Nicolas Sandeau for his contribution to the numerical simulation. We acknowledge financial support from the French Ministry of Research, the Centre National de la Recherche Scientifique (CNRS), the European Union (grant CARSExplorer FP7 Health and Micro-CARS COST MP603), and the land area "Provence-Alpes Côte d'Azur."

References

1. C. L. Evans and X. S. Xie, "Coherent anti-Stokes Raman scattering microscopy: Chemical imaging for biology and Medicine," *Annu. Rev. Anal. Chem.* **1** 883–909 (2008).
2. C. W. Freudiger, W. Min, B. G. Saar, S. Lu, G. R. Holtom, C. He, J. C. Tsai, J. X. Kang, and X. S. Xie, "Label-free biomedical imaging with high sensitivity by stimulated Raman scattering microscopy," *Science* **322** 1857–1861 (2008).
3. M. D. Duncan, J. Reintjes, and T. J. Manuccia, "Scanning coherent anti-Stokes Raman scattering microscope," *Opt. Lett.* **7** 350–352 (1982).
4. A. Zumbusch, G. R. Holtom, and X. S. Xie, "Three-dimensional vibrational imaging by coherent anti-stokes Raman scattering," *Phys. Rev. Lett.* **82** 4142–4145 (1999).
5. E. Ploetz, S. Laimgruber, S. Berner, W. Zinth, and P. Gilch, "Femtosecond stimulated Raman microscopy," *Appl. Phys. B* **87** 389–393 (2007).
6. Y. Ozeki, F. Dake, S. Kajiyama, K. Fukui, and K. Itoh, "Analysis and experimental assessment of the sensitivity of stimulated Raman scattering microscopy," *Opt. Express* **17** 3651–3658 (2009).
7. P. Nandakumar, A. Kovalev, and A. Volkmer, "Vibrational imaging based on stimulated Raman scattering microscopy," *New J. Phys.* **11** 033026 (2009).
8. A. Volkmer, L. D. Book, and X. S. Xie, "Time-resolved coherent anti-Stokes Raman scattering microscopy: Imaging based on Raman free induction decay," *Appl. Phys. Lett.* **80** 1505–1507 (2002).
9. E. O. Potma, C. L. Evans, and X. S. Xie, "Heterodyne coherent anti-Stokes Raman scattering (CARS) imaging," *Opt. Lett.* **31** 241–243 (2006).
10. N. Dudovich, D. Oron, and Y. Silberberg, "Single-pulse coherently controlled nonlinear Raman spectroscopy and microscopy," *Nature (London)* **418** 512–514 (2002).
11. S.-H. Lim, A. G. Caster, O. Nicolet, and S. R. Leone, "Chemical imaging by single pulse interferometric coherent anti-Stokes Raman scattering microscopy," *J. Phys. Chem. B* **110** 5196–5204 (2006).
12. F. Ganikhanov, C. L. Evans, B. G. Saar, and X. S. Xie, "High-sensitivity vibrational imaging with frequency modulation coherent anti-Stokes Raman scattering (FM CARS) microscopy," *Opt. Lett.* **31** 1872–1874 (2006).
13. M. Jurna, J. P. Korterik, C. Otto, J. L. Herek, and H. L. Offerhaus, "Vibrational phase contrast microscopy by use of coherent anti-Stokes Raman scattering," *Phys. Rev. Lett.* **103** 043905 (2009).
14. J.-X. Cheng, L. D. Book, and X. S. Xie, "Polarization coherent anti-Stokes Raman scattering microscopy," *Opt. Lett.* **26** 1341–1343 (2001).
15. A. Volkmer, J.-X. Cheng, and X. S. Xie, "Vibrational imaging with high sensitivity via epidected coherent anti-Stokes Raman scattering microscopy," *Phys. Rev. Lett.* **87** 023901 (2001).
16. J.-X. Cheng, A. Volkmer, and X. S. Xie, "Theoretical and experimental characterization of anti-Stokes Raman scattering microscopy," *J. Opt. Soc. Am. B* **19** 1363–1375 (2002).
17. V. V. Krishnamachari and E. O. Potma, "Focus-engineered coherent anti-Stokes Raman scattering microscopy: A numerical investigation," *J. Opt. Soc. Am. A* **24** 1138–1147 (2007).
18. V. V. Krishnamachari and E. O. Potma, "Imaging chemical interfaces perpendicular to the optical axis with focus-engineered coherent anti-Stokes Raman scattering microscopy," *Chem. Phys.* **341** 81–88 (2007).

19. V. V. Krishnamachari and E. O. Potma, "Multi-dimensional differential imaging with FE-CARS microscopy," *Vibr. Spectrosc.* **50** 10–14 (2009).
20. D. Gachet, S. Brustlein, and H. Rigneault, "Revisiting the Young's double slit experiment for background-free nonlinear Raman spectroscopy and microscopy," *Phys. Rev. Lett.* **104** 213905 (2010).
21. D. Gachet, F. Billard, and H. Rigneault, "Focused field symmetries for background-free coherent anti-Stokes Raman spectroscopy," *Phys. Rev. A* **77** 061802(R) (2008).
22. D. Gachet, F. Billard, and H. Rigneault, "Background-free coherent anti-Stokes Raman spectroscopy near transverse interfaces: a vectorial study," *J. Opt. Soc. Am. B* **25** 1655–1666 (2008).
23. H. Lotem, R. T. Lynch, and N. Bloembergen, "Interference between Raman resonances in four-wave difference mixing," *Phys. Rev. A* **14** 1748–1755 (1976).
24. G. W. H. Wurpel, J. M. Schins, and M. Müller, "Direct measurement of chain order in single phospholipid mono- and bilayers with multiplex CARS," *J. Phys. Chem. B* **108** 3400–3403 (2004).
25. D. Schafer, J. A. Squier, J. van Maarseveen, D. Bonn, M. Bonn, and M. Müller, "In situ quantitative measurement of concentration profiles in a microreactor with submicron resolution using multiplex CARS microscopy," *J. Am. Chem. Soc.* **130** 11592–11593 (2008).
26. D. Gachet and H. Rigneault, "Detection of chemical interfaces in conventional Coherent anti-Stokes Raman Scattering (CARS) microscopy," *J. Opt. Soc. Am.* (submitted).